Imaging Agents

DOI: 10.1002/anie.201201661

Fluorochrome-Functionalized Magnetic Nanoparticles for High-Sensitivity Monitoring of the Polymerase Chain Reaction by Magnetic Resonance**

*David Alcantara, Yanyan Guo, Hushan Yuan, Craig J. Goergen, Howard H. Chen, Hoonsung Cho, David E. Sosnovik, and Lee Josephson**

DNA generated by the polymerase chain reaction (PCR DNA) is normally detected by fluorescence; however, with the development of small magnetic resonance (MR) relaxometers[1] and magnetic nanoparticle/magnetic relaxation switch assays,[2] detection of the PCR reaction by MR might provide an alternative to fluorescence. We hypothesized that a magnetic nanoparticle (NP) surface-functionalized with multiple DNA-binding fluorochromes would react with DNA, forming multivalency-driven microaggregates and allowing for a high-sensitivity detection of PCR-generated DNA by MR. Binding of DNA to solid phases is usually based on electrostatic interactions between a surface functionality and negatively charged phosphates on DNA[3] or by base-pairing with surface oligonucleotides.[2a,4] Surface functionalization of NPs with DNA-binding fluorochromes is a new approach for design of surfaces for DNA detection. Our study then combines three key elements: 1) the synthesis of fluorochrome mediated, DNA binding surfaces; 2) the reaction of fluorochrome functionalized NPs with DNA to form microaggregates at low DNA concentrations; and 3) the detection of microaggregates formed by the reaction of the NP with PCR-generated DNA by MR relaxometry or MRI.

We attached the DNA-binding fluorochrome TO-PRO 1 to the Feraheme (FH) NP by reacting TO NHS[5] with amino-Feraheme[6] (Figure 1a) to yield a NP denoted FH-TO. Approved for treating iron anemia, FH has a publically available formula ($Fe_{5874}O_{8752}$) with 414 carboxyl groups owing to its carboxymethyl dextran coating.[7] The FH-TO had 9.9 ± 2.4 TO-PRO 1 per NP (per 5874 iron atoms) attached through a six-carbon linker. (Values are the means ± 1 SE, $n = 4$). FH-TO had r_1 and r_2 relaxivities of 23.3 ± 2.2 and 122 ± 12 mM Fe^{-1}, respectively (0.47T, 40°C), and a size of 59.8 ± 3.4 nm (intensity weighted by dynamic light scattering). The FH had a zeta potential of -37.8 ± 3 mV at pH 6 that was largely preserved with the attachment of 9.9 TO-PRO 1; the zeta potential of FH-TO was still highly negative (-28.3 ± 0.8 mV). Preservation of a negative NP surface prevents electrostatic binding between a negatively charged DNA and a positively charged NP and insures that when FH-TO binds to DNA, it does so with an intercalation mechanism (Figure 1b) with a generation of fluorescence.

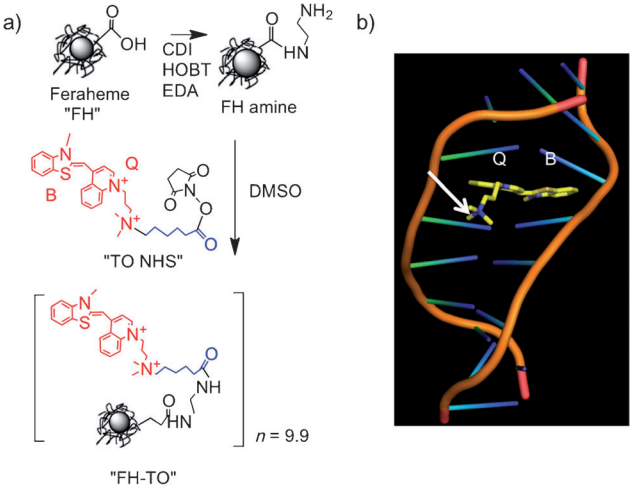

Figure 1. Synthesis of the FH-TO NP and TO-PRO 1 intercalation with DNA. a) An NHS ester of TO-PRO 1 ("TO NHS") was reacted with aminated Feraheme (FH amine) to yield FH-TO with 9.9 TO per NP. CDI = carbodiimide, EDA = ethylene diamine, HOBT = hydroxybenzotriazole. "TO NHS" consists of TO-PRO 1 (red), a six-carbon linker (blue), and an NHS ester. b) Model showing benzathiazole (B) and quinoline (Q) rings of TO-PRO 1 (TO) intercalating into DNA. With TO NHS, a linker (not shown in (b)) maintains the quarternary positive charge (arrow) and does not interfere with the intercalation of the B and Q rings.

The interactions of the magnetofluorescent FH-TO NP with increasing concentrations of λ DNA, and two synthetic oligonucleotides (18 and 10 base pair (bp)), were examined using transverse MR relaxation times (ΔT2; Figure 2a) and fluorescence intensities (Figure 2b). Both gave hyperbolic functions with well-defined maxima, but the FH-TO/ΔT2 response occurred at far lower DNA concentrations. Our

[*] Dr. D. Alcantara, Dr. Y. Guo, Dr. H. Yuan, Dr. H. Cho, Prof. Dr. D. E. Sosnovik, Prof. Dr. L. Josephson
Center for Translational Nuclear Medicine and Molecular Imaging
Massachusetts General Hospital
149 13th Street, Charlestown, MA 02129 (USA)
E-mail: ljosephson@mgh.harvard.edu
Dr. D. Alcantara
Instituto de Nanociencia de Aragon, Universidad de Zaragoza
50018 Zaragoza (Spain)
Dr. C. J. Goergen, Dr. H. H. Chen, Prof. Dr. D. E. Sosnovik, Prof. Dr. L. Josephson
Martinos Center for Biomedical Imaging
Massachusetts General Hospital
149 13th Street, Charlestown, MA 02129 (USA)

[**] This work was funded by NIH grants R01 EB009691 and R01 EB011996 to L.J. and R01 HL093038 (D.E.S.). D.A. was a recipient of a Marie Curie Fellowship (IOF, MRI Nanobiosensor).

Supporting information for this article is available on the WWW under http://dx.doi.org/10.1002/anie.201201661.

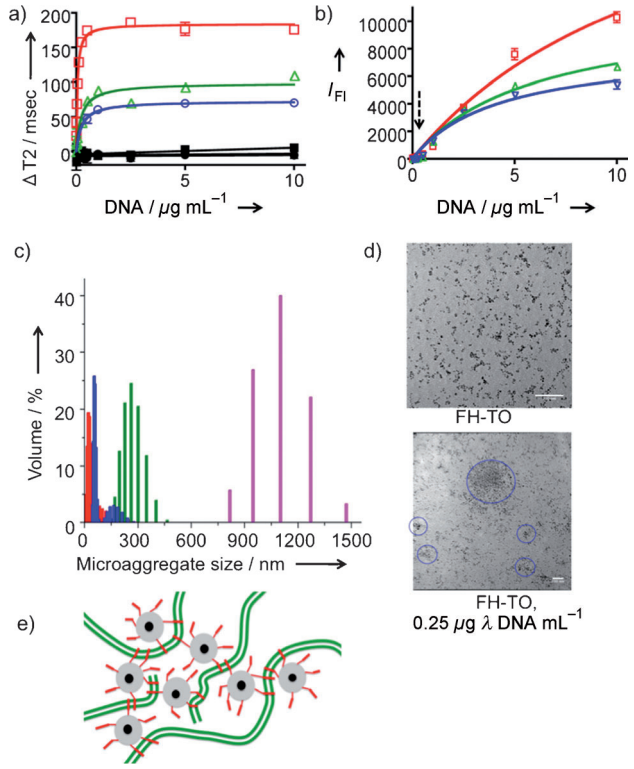

Figure 2. The reaction of FH-TO with DNA as followed by T2, fluorescence, and light scattering. a) Changes in T2 (ΔT2) and b) fluorescence (I_{FI}) for FH-TO with increasing concentrations of λ DNA, 18 bp, and 10 bp oligonucleotides. ΔT2 = T2 (FH,DNA) − T2(FH-TO,DNA); λ DNA (□), 18 bp oligo (△), 10 bp oligo (○). The lack of T2 response with FH is also indicated in (a) (black symbols). Data was fit to single site binding model, yielding the apparent dissociation constants K_d (Table 1). The dotted arrow in (b) indicates a concentration of 0.25 μg mL^{-1} DNA, at which fluorescence is very low. At this concentration, microaggregates were detected by dynamic light scattering (c); key: FH-TO only (red), and with 0.007 (blue), 0.25 (green), and 1 μg mL^{-1} DNA (magenta). Microaggregates were also confirmed by TEM (d); scale bar 100 nm. e) Model of microaggregate formation of FH-TO and DNA. Microaggregates form with very few of the TO-PRO 1 (red) on the FH-TO NP (gray = carboxymethyl dextran coating, black = iron oxide core) intercalating with double stranded DNA (green).

three DNAs did not react with the control FH NP (Figure 2a), showing that the FH-TO/DNA interaction was mediated by TO-PRO 1, which fluoresces when intercalated between the bases of double-stranded DNA.[8] The curves were then fitted to a single site-binding model, yielding the apparent K_d values summarized in Table 1. At concentrations between 0 and 0.25 μg mL^{-1} of λ DNA, values that were at least ten times lower than any of the K_d values obtained by fluorescence, FH-TO formed microaggregates evident by light scattering (Figure 2c) and TEM (Figure 2d). The formation of microaggregates of FH-TO and target DNA molecules exploits multivalent interactions between the 9.9 TOs on the FH-TO surface and numerous intercalation sites on polymeric DNA (Figure 2e). Our model proposes that FH-TO/DNA microaggregates form through TO intercalation and fluorescence (Figure 1b and above), as indicated by the failure of DNA to react with FH (Figure 2a and Figure 3a). Second, FH-TO/DNA microaggregates form with only small fraction of the TOs on FH-TO surface involved in the DNA intercalation, which generates fluorescence (Figure 2e). Thus the K_d values by ΔT2 were well below those for fluorescence with all three DNAs examined (Table 1). Finally, as longer DNA provides more sites for intercalation, and thus for multivalent interactions with FH-TO, microaggregate-based, ΔT2 K_d values were dependent on the size of the DNA target, decreasing (exhibiting higher affinity) as target molecular weight increased (Table 1). Alternatively, K_d values can be expressed as molar concentrations by using the K_d values and molecular weights provided in Table 1.

Table 1: Apparent affinities for FH-TO and DNAs by relaxometry (K_d,ΔT2) and fluorescence (K_d,I_{FI}).

DNA & MW [kDa]	Compound	K_d, ΔT2 [μg mL^{-1}]	K_d, I_{FI} [μg mL^{-1}]	K_d,I_{FI}/ K_d,ΔT2
λ DNA, 31 500	FH-TO	0.050	13.5	270
18 bp, 10.99	FH-TO	0.232	5.93	25.5
10 bp, 6.05	FH-TO	0.253	4.19	16.6
λ DNA	TO-PRO 1		3.19	
18 bp	TO-PRO 1		3.29	
10 bp	TO-PRO 1		4.17	

We next examined the ability of FH-TO to detect DNA by adding the NP to a model cycling PCR reaction, and by obtaining T2 using the phantom design (Supporting Information, Figure S1) and determining T2 by imaging (Figure 3a). With a full complement of PCR reagents, T2 relaxation times increased with cycle number (CN), a response not seen with no DNA template (FH-TO/-T) or with PCR reagents and template but with a NP lacking TO-PRO 1 (FH/+T). As the change in MR signal was dependent on the presence of DNA template and the TO-PRO 1 surface functionalization of FH, FH-TO reacts with the DNA produced by the PCR reaction, and that reaction permits DNA to be imaged by MR. The reaction of FH-TO with PCR generated DNA at 1–15 cycles was then examined by microaggregate formation (light scattering) and T2 changes by relaxometry (Figure 3b). After a single cycle, FH-TO reacted with PCR primers to form microaggregates (microaggregates = 402 nm, FH-TO = 59 nm), and these grew in size with increasing cycle numbers. Thus PCR generated DNA and FH-TO formed microaggregates, with changes in T2 by MRI (9.4T, Figure 3a) or relaxometry (Figure 3b). The responses to PCR generated DNA by MRI (9.4T, Figure 3a), relaxometry (0.47T, Figure 3b) were compared with responses obtained with SybrGreen of FH-TO fluorescence as shown using the logit equation (Figure 3c; raw data provided in the Supporting Information, Table S1). Fluorescence was far less sensitive at detecting the PCR reaction than T2 by MRI (Figure 3a) or relaxometry (Figure 3b). Finally, we determined the sensitivity of detection of PCR generated DNA by T2 relaxometry and fluorescence by using PCR reactions run with various amounts of template DNA (Figure 3d). Over a wide range of DNA template amounts, the detection thresholds (Ct) determined using FH-TO and T2 were substantially lower than Ct values determined by SybrGreen fluorescence. (Ct = 20% of maximum signal change for fluorescence or MR.) The

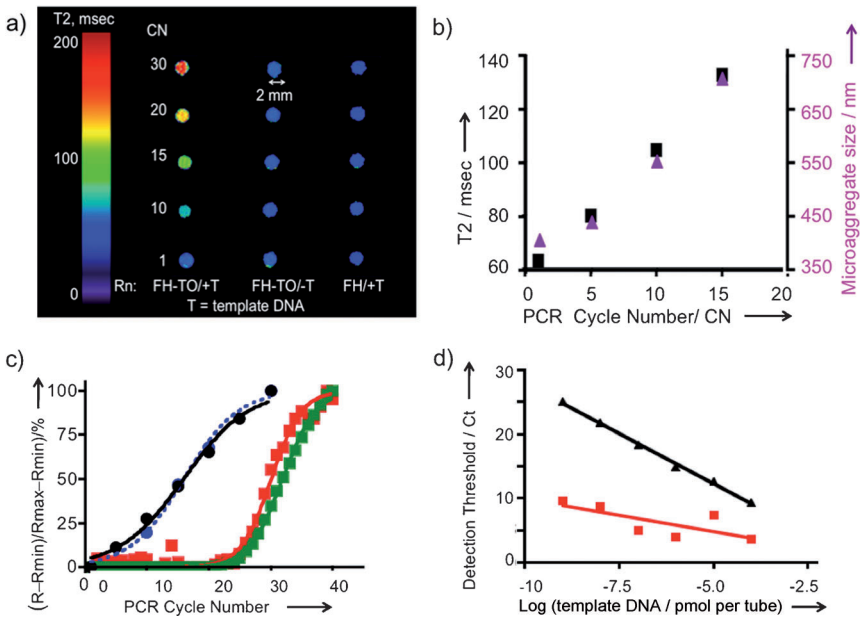

Figure 3. Monitoring PCR-produced DNA by MR. a) PCR reactions with added FH-TO were run in sealed PCR tubes, placed in a Gd-DTPA solution to minimize air/solution artifacts (Supporting Information, Figure S1), and imaged by MR at 9.4T. T = template DNA. Rn = reaction conditions. Omission of template DNA or use of Feraheme (FH), rather than FH-TO, yielded no changes in T2. b) The PCR reaction was repeated and tubes were opened for measurements of T2 using a 0.47T relaxometer and microaggregate size (by light scattering). FH-TO (59 nm) reacted with primers to form microaggregates (402 nm) after one PCR cycle. At higher cycle numbers, microaggregate size and T2 increased. c) Comparison of the response by T2 and fluorescence with increasing cycle numbers. 0.47T data (●) are from (b), while 9.4T data (●) are from (a). Fluorescence was determined using SybrGreen (■) and FH-TO (■) as fluorochromes. d) Comparison of threshold cycle (Ct) by fluorescence (▲) and T2 (■) as a function of template DNA amounts. Ct values from T2 are lower than those fluorescence because microaggregate formation is being measured, which occurs with little or no fluorescence (Figure 2e).

lower Ct values by T2 result from a multivalent reaction between the surface of FH-TO (9.9 TOs/NP) and PCR-generated DNA, which forms microaggregates, a reaction that occurs at cycle numbers where fluorescence has not yet changed (CN = 1 to 15; see microaggregate size from Figure 3b).

To determine whether FH-TO and MR could be used in a widely employed PCR application, cDNA from apoptotic Jurkat T cells was added to a commercially available, RT-PCR apoptosis-related gene expression array. At cycle 32, tubes with widely varying fluorescences from Figure 4a were selected, split into two portions with FH-TO or FH added, and the difference in T2 values determined by relaxometer; the correspondence between fluorescence and ΔT2 obtained is shown in Figure 4b. The correspondence is only approximate, reflecting for example the fact that PCR-generated DNA can have variable molecular weights and form microaggregates in a manner that does not completely parallel fluorochrome intercalation and fluorescence. Note the dependence of K_d on DNA molecular weight (Table 1.)

Finally, we added FH-TO or FH to apoptosis expression arrays which were stopped first at CN = 18, a point where the fluorescent response was initiated (Figure 4a), and then at 32 cycles, a point where there was high and variable fluorescence (for fluorescence data for the full array, see the Supporting Information, Figure S2). MR images of the plates were made as a function of cycle number and NP (FH vs. FH-TO; Figure 4c). With the non-DNA binding FH at CN = 18 (or CN = 32, not shown), all wells had T2 values of about 110–120 ms (orange to yellow), indicating no reaction with the non-fluorochrome-bearing control NP. On the other hand, at CN = 18 and with the DNA binding FH-TO, the T2 values of some wells (A1, B2) were lower (more bluish) than those with FH. With FH-TO and at CN = 32, T2 changes were greater; some wells had lower (B5, B6) and some higher T2 values than the FH control, (B1, B2). FH-TO, and not FH, reacted with products of a RT-PCR reaction in a cycle-dependent fashion. The detection of FH-TO/DNA microaggregates by MR has been achieved in a simple mix-and-read format (Figure 2), with a model PCR reaction (Figure 3), and with a commercial RT-PCR array for determining mRNA levels of apoptosis-related genes (Figure 4).

When FH-TO reacts with DNA, T2 can decrease (Figure 2a) or increase (Figure 3a) or can vary from well to well, as in the array (Figure 4c, CN = 32 B1, B2: T2 increase; B5, B6: T2 decrease). The differing effects of magnetic NP aggregation on T2 has been observed before[9] and are explained by magnetic sphere relaxation theory. When small dispersed NPs like FH-TO form microaggregates, larger magnetic field inhomogeneities are produced; these are more efficient dephasers of the T2 relaxation process and T2 decreases with microaggregate formation. When very large micrometer-sized aggregates are formed, a diffusion-limited condition results and T2 increases with further aggregation.[10] With PCR arrays, T2 readings at multiple cycle numbers might therefore be needed to yield unambigious values of the relative mRNAs determined by the RT-PCR method.

Surface functionalization with nucleic acid binding fluorochromes offers a potentially general strategy for the design of nucleic acid binding nanoparticles. Elements of our strategy are: 1) select a nucleic acid binding fluorochrome and synthesize its NHS ester with a linker placed so as not to impair DNA binding (impaired DNA binding can be assessed with an in vitro DNA binding fluorescence assay); 2) synthesize a surface functionalized, multivalent nanoparticle; and 3) employ the multivalent NP in a solution phase, multivalent reaction where it forms microaggregates with a target DNA, a formation which can be monitored by T2, light scattering, or other microaggregate detection techniques.

Further improvements in sensitivity of T2-based detection may be possible through the use of larger magnetic particles

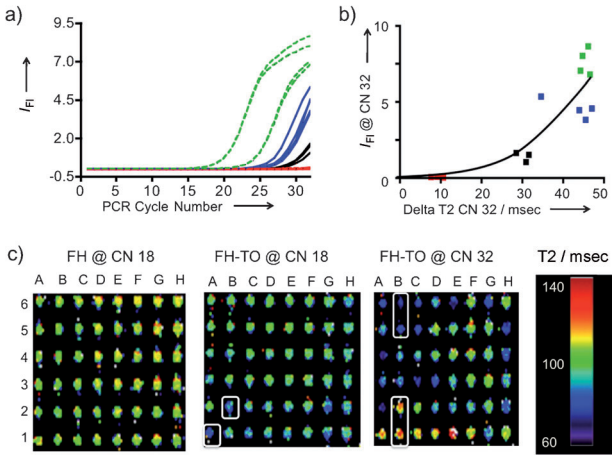

Figure 4. Detection of apoptosis-related gene expression by RT-PCR using FH-TO and MR. a) The RT-PCR reaction was monitored by fluorescence. Gene expression was classified as high (green), medium (blue), low (black), or very low (red). Reaction was stopped at 32 cycles to maximize the differences in fluorescence. The fluorescence response for all genes and over the entire cycle range is shown in the Supporting Information, Figure S2. FH-TO or FH was then added at CN = 32 and delta T2 values determined by relaxometry. b) Comparison of fluorescence from (a) with ΔT2 values by relaxometry. Data was fitted to the hyperbolic equation $y = 0.2551^{0.07007x}$; $r^2 = 0.76$. c) MRI of the apoptosis-related gene expression with FH-TO (or FH control). At CN = 18 and FH addition, all wells were between 100 and 140 ms. At CN = 18, FH-TO the A1 and B2 wells had lower T2s (more bluish), indicating PCR DNA production. At CN = 32, some FH-TO wells have lower (B5, B6) and have higher T2 values than the FH control (B1,B2). FH-TO, and not FH, reacts with products of the RT-PCR reaction in a cycle-dependent fashion.

or magnetic-field-assisted NP aggregation, techniques that have resulted in substantial improvements in sensitivity with the detection of antibodies by relaxometry.[9] A higher sensitivity of DNA detection can reduce the number of PCR cycles used to detect templates, reducing amplification related errors, while the ability to measure T2 within enclosed reaction tubes can eliminate post-amplification contamination. When combined with recent advances in miniature relaxometers noted above, the detection of PCR-generated DNA in sealed reaction tubes (Figure 3b), and at high sensitivity (Table 1, Figure 2a, 3d), may permit the use of the PCR method in settings where it is not now possible.

Received: March 1, 2012
Revised: April 4, 2012
Published online: June 8, 2012

Keywords: fluorescence · imaging agents · magnetic nanoparticles · magnetic resonance imaging · polymerase chain reaction

[1] a) J. B. Haun, T. J. Yoon, H. Lee, R. Weissleder, *Methods Mol. Biol.* **2011**, *726*, 33–49; b) H. Lee, E. Sun, D. Ham, R. Weissleder, *Nat. Med.* **2008**, *14*, 869–874; c) J. Bart, J. W. Janssen, P. J. van Bentum, A. P. Kentgens, J. G. Gardeniers, *J. Magn. Reson.* **2009**, *201*, 175–185; d) H. Wensink, F. Benito-Lopez, D. C. Hermes, W. Verboom, H. J. Gardeniers, D. N. Reinhoudt, A. van den Berg, *Lab Chip* **2005**, *5*, 280–284.

[2] a) L. Josephson, J. M. Perez, R. W. Weissleder, *Angew. Chem.* **2001**, *113*, 3304–3306; *Angew. Chem. Int. Ed.* **2001**, *40*, 3204–3207; b) J. M. Perez, L. Josephson, R. Weissleder, *ChemBioChem* **2004**, *5*, 261–264; c) J. B. Haun, T. J. Yoon, H. Lee, R. Weissleder, *Wiley Interdiscip. Rev. Nanomed. Nanobiotechnol.* **2010**, *2*, 291–304.

[3] a) M. A. Marko, R. Chipperfield, H. C. Birnboim, *Anal. Biochem.* **1982**, *121*, 382–387; b) R. Boom, C. J. Sol, M. M. Salimans, C. L. Jansen, P. M. Wertheim-van Dillen, J. van der Noordaa, *J. Clin. Microbiol.* **1990**, *28*, 495–503.

[4] a) T. Maruyama, T. Hosogi, M. Goto, *Chem. Commun.* **2007**, 4450–4452; b) T. Ito, C. L. Smith, C. R. Cantor, *Proc. Natl. Acad. Sci. USA* **1992**, *89*, 495–498; c) N. L. Rosi, D. A. Giljohann, C. S. Thaxton, A. K. Lytton-Jean, M. S. Han, C. A. Mirkin, *Science* **2006**, *312*, 1027–1030; d) J. M. Perez, L. Josephson, T. O'Loughlin, D. Hogemann, R. Weissleder, *Nat. Biotechnol.* **2002**, *20*, 816–820.

[5] a) E. Garanger, S. A. Hilderbrand, J. T. Blois, D. E. Sosnovik, R. Weissleder, L. Josephson, *Chem. Commun.* **2009**, 4444–4446; b) S. Huang, H. H. Chen, H. Yuan, G. Dai, D. T. Schuhle, C. Mekkaoui, S. Ngoy, R. Liao, P. Caravan, L. Josephson, D. E. Sosnovik, *Circ. Cardiovasc. Imaging* **2011**, *4*, 729–737.

[6] S. Chen, D. Alcantara, L. Josephson, *J. Nanosci. Nanotechnol.* **2011**, *11*, 3058–3064.

[7] a) W. Li, S. Tutton, A. T. Vu, L. Pierchala, B. S. Li, J. M. Lewis, P. V. Prasad, R. R. Edelman, *J. Magn. Reson. Imaging* **2005**, *21*, 46–51; b) V. S. Balakrishnan, M. Rao, A. T. Kausz, L. Brenner, B. J. Pereira, T. B. Frigo, J. M. Lewis, *Eur. J. Clin. Invest.* **2009**, *39*, 489–496.

[8] a) L. Van Hove, W. Goossens, V. Van Duppen, R. L. Verwilghen, *Clin. Lab. Haematol.* **1990**, *12*, 287–289; b) J. Nygren, N. Svanvik, M. Kubista, *Biopolymers* **1998**, *46*, 39–51; c) A. N. Glazer, H. S. Rye, *Nature* **1992**, *359*, 859–861; d) S. Prodhomme, J. P. Demaret, S. Vinogradov, U. Asseline, L. Morin-Allory, P. Vigny, *J. Photochem. Photobiol. B* **1999**, *53*, 60–69.

[9] a) R. Hong, M. J. Cima, R. Weissleder, L. Josephson, *Magn. Reson. Med.* **2008**, *59*, 515–520; b) I. Koh, R. Hong, R. Weissleder, L. Josephson, *Angew. Chem.* **2008**, *120*, 4187–4189; *Angew. Chem. Int. Ed.* **2008**, *47*, 4119–4121; c) I. Koh, R. Hong, R. Weissleder, L. Josephson, *Anal. Chem.* **2009**, *81*, 3618–3622.

[10] a) R. N. Muller, P. Gillis, F. Moiny, A. Roch, *Magn. Reson. Med.* **1991**, *22*, 178–182; b) R. A. Brooks, F. Moiny, P. Gillis, *Magn. Reson. Med.* **2001**, *45*, 1014–1020.

